Energetic Heavy-Ion and Proton Generation from Ultraintense Laser-Plasma Interactions with Solids

E. L. Clark,[1,2] K. Krushelnick,[1] M. Zepf,[1] F. N. Beg,[1] M. Tatarakis,[1] A. Machacek,[3] M. I. K. Santala,[1] I. Watts,[1] P. A. Norreys,[4] and A. E. Dangor[1]

[1]*Imperial College of Science, Technology and Medicine, London SW7 2BZ, United Kingdom*
[2]*Radiation Physics Department, AWE, Aldermaston, Reading, RG7 4PR, United Kingdom*
[3]*Department of Physics, University of Oxford, Oxford, OX1 3PU, United Kingdom*
[4]*Rutherford Appleton Laboratory, Chilton, Oxon, OX11 0QX, United Kingdom*

(Received 9 November 1999)

Heavy ions with energies up to 430 ± 40 MeV have been measured from laser-solid interactions at focused intensities of up to 5×10^{19} W/cm^2. Observations of proton emission indicate significant structure in the energy spectrum as well as an angular emission profile which varies with energy. Two qualitatively different components of ion emission are observed: (i) a high-energy component which is likely generated by a combination of "Coulomb explosion" and acceleration by the space charge force from hot electrons which escape the plasma, and (ii) a lower-energy component which forms a ring likely created by magnetic fields in the ablated plasma.

PACS numbers: 52.40.Nk, 29.30.Ep, 52.70.Nc

Recent ultraintense laser-plasma interaction experiments have produced observations of many interesting new phenomena—such as the acceleration of electrons to energies of up to 100 MeV [1], the production of intense, directional proton beams [2], and the generation of multimegagauss magnetic fields [2,3]. Such developments may one day allow construction of compact tabletop particle accelerators with applications for high-energy physics and medicine. This work has been made possible by the implementation of chirped pulse amplification (CPA) technology in modern laser facilities, which can currently achieve focused intensities approaching 10^{21} W/cm^2. Under these conditions intense electron beams can be produced [4]—which may be useful for igniting compressed deuterium-tritium capsules in inertial confinement fusion experiments [5]. The physical mechanisms which produce these high-energy electrons are also important for understanding the generation of very energetic ions observed during laser interactions with dense plasmas [2,6,7]. The first measurements of energetic ion emission were made during early experiments [8] using CO_2 lasers and those results [9,10] indicated that ions with energies greater than 2 MeV/nucleon could be produced. Ions produced from intense laser-plasma interactions may also prove to be useful in a variation of the "fast ignitor" scheme [5].

This Letter reports detailed measurements of very energetic ions produced from the interaction of ultraintense lasers pulses with solid-density materials. Energy spectra of heavy ions and protons were recorded with high spatial and spectral resolution from the front of the target and exhibit novel features which can be linked to ion acceleration mechanisms in the plasma. We report here the highest-energy ions observed from a laser-produced plasma with measurements of Pb^{46+} ions up to 430 ± 40 MeV as well as protons with energies up to 30 MeV. Two components to the ion emission have been observed. We have observed the formation of lower-energy ring structures composed of protons and heavier ions (<4 MeV/nucleon) which may be caused by self-generated magnetic fields in the expanding plasma. The higher-energy component, however, displays different spatial characteristics, suggesting that these ions may have been accelerated by a combination of a "Coulomb explosion" during the time of the laser interaction and a subsequent acceleration by the hot electrons which escape the plasma [11].

These experiments were carried out at the Rutherford Appleton Laboratory using the VULCAN laser [12] which produces pulses having energies of up to 50 J at a wavelength of 1.053 μm and temporal duration of 0.9–1.2 ps. The laser beam was p polarized and was focused onto a thin target with a $f/4$ off-axis parabolic mirror at an incident angle of 45° from the target normal. The maximum intensity on target, up to 5×10^{19} W/cm^2, was determined from simultaneous measurements of the pulse energy, spot size, and pulse duration. The density scale length of the preplasma at the target surface, caused by the inherent prepulse in the laser (which was about 10^{-6} of the main pulse), was measured by optical probing and was typically found to be less than 10 μm. Ion emission was measured from the front of the target. To measure both the heavy-ion and proton spectra, a Thomson parabola ion spectrometer (Fig. 1) using CR39 plastic nuclear track detectors was situated at an angle of 20° from the target normal. In addition, the energy spectrum and spatial distribution of protons emitted from the interaction was determined by placing a stack of several pieces of radiochromic film (which is sensitive to ionizing radiation) and CR39 detectors in front of the target.

The laser was initially incident on 2 mm thick, 10 × 10 mm area, lead targets. Ions were collimated by a 250 μm diameter pinhole prior to traveling through the

 0031-9007/00/85(8)/1654(4)$15.00

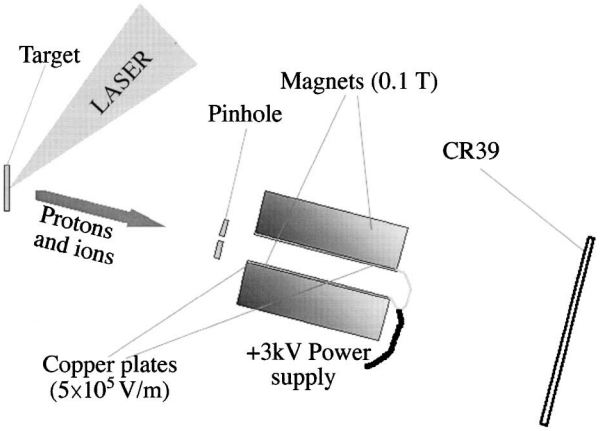

FIG. 1. Schematic of the experimental setup.

Thomson parabola spectrometer. Ions having a particular charge-to-mass ratio are deflected in the spectrometer so that they describe a unique parabola on the detector plane where a CR39 nuclear track detector (1 mm thick) is placed. CR39 is sensitive to ions and protons with energies greater than 100 keV/nucleon so this instrument is able to measure protons in the range from 100 keV to 11 MeV and heavy ions (carbon, lead, aluminum) having energies as much as several hundred MeV.

Figure 2 shows spectra derived from the Thomson parabola for a lead target. Parabolas on the CR39 can be easily identified as carbon with charge states up to C^{6+} together with a proton parabola. Measurements reveal "band"-like structures in the energy spectrum of the carbon ions as well as large modulations in the number of protons as a function of energy. In particular, several bands were routinely observed in each carbon spectrum, with each band occurring at the same velocity for the different charge states. In the Fig. 2 inset, the spectrum for the C^{6+} ions is plotted on a linear scale and clearly demonstrates the highly modulated nature of the spectrum. A proton spectrum (Fig. 3) taken from the Thomson parabola shows multiple peaks which vary in intensity and position between shots in a similar way as the bands observed in the heavy-ion spectra. This proton spectrum also shows two distinct populations with a "flattening" of the spectrum at about 4 MeV.

Electrons propagating away from the target in the ablated plume of plasma can accelerate ions forming an electrostatic sheath [13] which results in a sharp cutoff in the ion spectrum. A "two-temperature" plasma has been previously observed to produce a dip in the energetic ion spectrum [14]—resulting in two distinct ion populations. A complex electron spectrum [15], similar to that measured in this experiment, is consequently likely to manifest itself as modulations in the ion spectra—as different populations of ions are accelerated to a particular "band" of energies.

Previous measurements [7,9,10] suggest that the principal component of the ion emission is protons; however, it is clear that a substantial contribution is due to

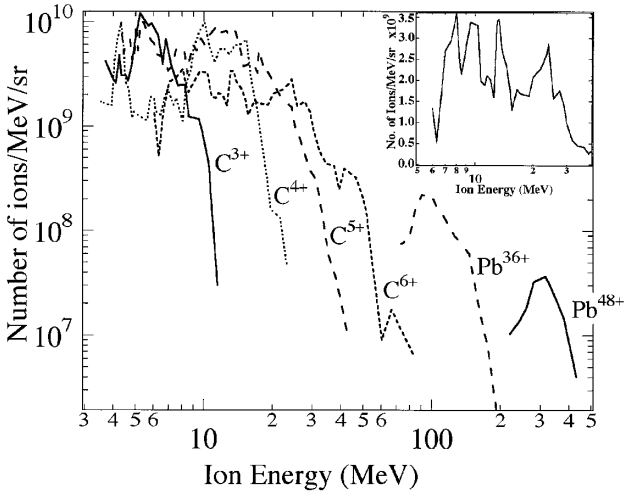

FIG. 2. Experimental spectra of carbon ions and lead ions from the same shot. The C^{6+} ion spectrum plotted on a linear scale is inset.

other ion species. Measurements of ion emission from lead targets (Fig. 2) indicate Pd-like Pb^{36+} ions up to 220 ± 30 MeV and Xe-like Pb^{46+} ions up to about 430 ± 40 MeV (closed shells). Fully stripped aluminum ions up to 150 ± 10 MeV and carbon ions 90 ± 10 MeV were also measured. The peak ion energy was observed to increase with the mass of the ion and its charge state. The fact that the most energetic heavy ions have the highest charge state suggests that part of the acceleration of the highest-energy ions is produced as each ion species falls through a similar potential—such as that set up near the critical surface. This results in the dependence of the final ion energy on the initial charge state. The increase in energy with Z is faster than expected because the ion recombination rate for heavy ions is inversely proportional

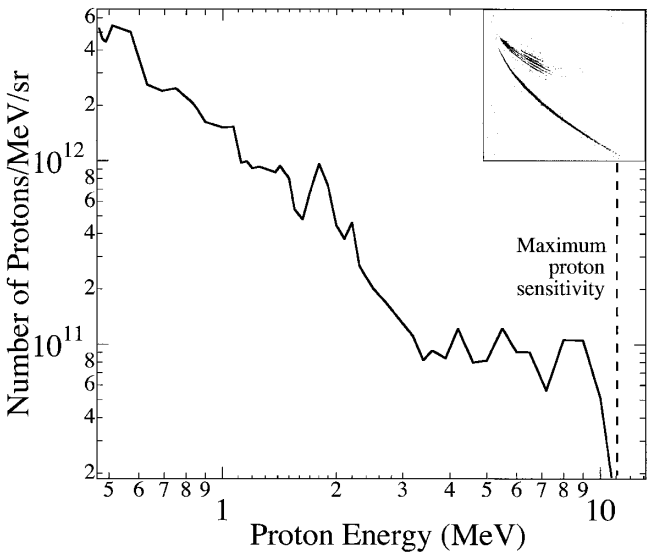

FIG. 3. Proton spectrum indicating multiple peaks and a flattening of the spectrum at ~4 MeV. Data from the Thomson parabola is inset.

to the ion velocity, making low-energy ions more likely to recombine to the lower ionization stages.

A plot of the maximum ion energy against $I\lambda^2$ ($\mathrm{W\,cm^{-2}\,\mu m^2}$) from data taken during these series of experiments is shown in Fig. 4 (squares) together with data from Refs. [7] and [10] (circles). Clearly, there are large shot-to-shot variations in the data over the entire range of intensities plotted from 10^{13} to 10^{20} $\mathrm{W\,cm^{-2}\,\mu m^2}$. However, least-squares fits to the data reveal two regimes. Up to 10^{18} $\mathrm{W\,cm^{-2}\,\mu m^2}$, the maximum ion energy scales as $(I\lambda^2)^{0.4}$ but when the oscillatory velocity of the fast electrons becomes relativistic (at about 10^{18} $\mathrm{W/cm^2}$), the maximum ion energy scales as $(I\lambda^2)^{0.5}$. It is likely that this scaling is a transition from classical resonance absorption to ponderomotive $\mathbf{J} \times \mathbf{B}$ absorption at relativistic intensities [16].

The spatial and spectral distribution of the ions was measured using a sandwich of radiochromic film (RCF) [17] and CR39 plastic track detectors. RCF is composed of nylon coated with an organic dye which increases in optical density when exposed to ionizing radiation. At the surface of the different layers of RCF/CR39 in this detector stack, protons having a particular range of energies release most of their energy just as they stop. Consequently, this produces a signal on the RCF/CR39 for only this range of energies. The stopping range of protons in radiochromic film and RCF/CR39 is well known—so, at a particular layer, the energy of protons producing the signal can be easily determined.

The CR39/radiochromic film detector stack was aligned parallel to the target at a distance of 45 mm from the surface so that the center of the stack coincided with the target normal. Each piece of CR39 was 5 × 5 cm. The target in this instance was a 125 μm thick piece of aluminum. No heavy ions can penetrate the first layer of radiochromic film so signal on the subsequent pieces of CR39 is largely due to energetic protons originating from hydrocarbon contaminants on the front surface of the target and in the target material—as observed in previous work [7,9,10].

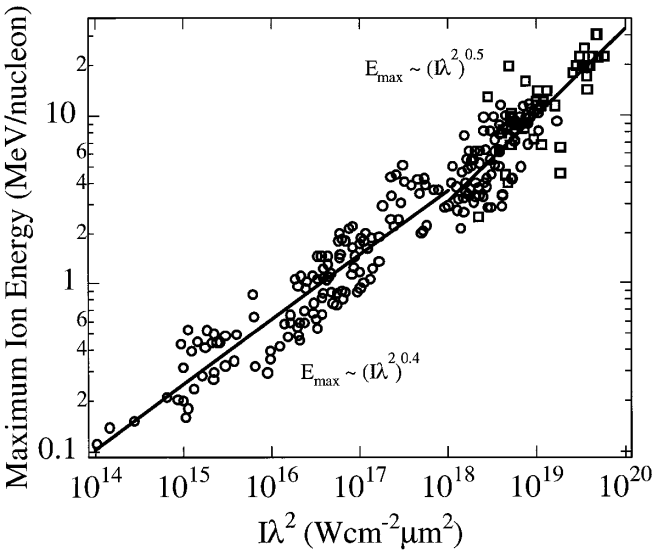

FIG. 4. Maximum ion energy as a function of $I\lambda^2$. Data from Refs. [7] and [10] are indicated by circles. Squares denote data from experiments discussed here.

Figure 5(a) is a typical image of the first piece of radiochromic film and Fig. 5(b) is an image of its rear surface. This shows a ring structure which is consistent with the ring of low-energy ($\leq$4 MeV) protons recorded on the following piece of CR39 [Fig. 5(c)] outside of which little additional signal can be seen. The center of the ring does not coincide with the target normal, but is shifted by about 10° towards the direction of the incident laser. Overall, the lowest-energy ion emission occurs within a 20° cone (the plasma plume) and shows a fine scale filamentary structure. An estimate of the number of protons within this ring indicates there are approximately 10^{12} with energies greater than 2 MeV. Common to Figs. 5(b) and 5(c) is a feature in the center which is caused by emission along the target normal.

Figures 5(d) and 5(f) show higher-energy protons measured by the subsequent pieces of CR39 in the stack which are separated by a single piece of radiochromic film. The average energies at these surfaces are 11 and 13 MeV, respectively. Here, no ring structure is observed and the protons cover an emission area which gets smaller as the energy increases, but has no apparent correlation with that at lower energies. Figures 5(g) and 5(h) show high-energy protons of 18 and 20 MeV observed in a subsequent shot, the spatial distributions of which have the same basic characteristics as those in Figs. 5(a)–5(f). Simultaneous measurements at the front and the rear [2] of the target indicate that the maximum proton energies are almost the same in both directions. The fact that the very highest-energy ions in the plasma plume have a similar energy to those recorded at the back of the target suggests that their acceleration mechanisms may be related.

It is likely that the lower-energy component of the ions is produced during the expansion of the plasma plume. During this period, temperature gradients along the target surface combined with nonparallel density gradients from the expanding plasma can produce self-generated magnetic fields [18]. Such magnetic fields can deflect the expanding plasma—forming the "plasma ring" which is subsequently recorded at low-energy protons and ions on the radiochromic film at shown in Figs. 5(a) to 5(c). Such plasma formation has been observed in MHD simulations and in previous experiments [3]. This ring may also be partly due to a density minimum in the plasma which is produced by the ponderomotive force associated with very high laser intensity [19]. The measured ions have energies that are consistent with plasma expansion velocities as measured by optical probing [20]. The magnetic pressure along the target normal from the self-generated magnetic field can collimate the expanding plasma at the laser spot to produce a jet of plasma containing low-energy ions and electrons. This can be seen as the central features in Figs. 5(b) and 5(c). Jets have

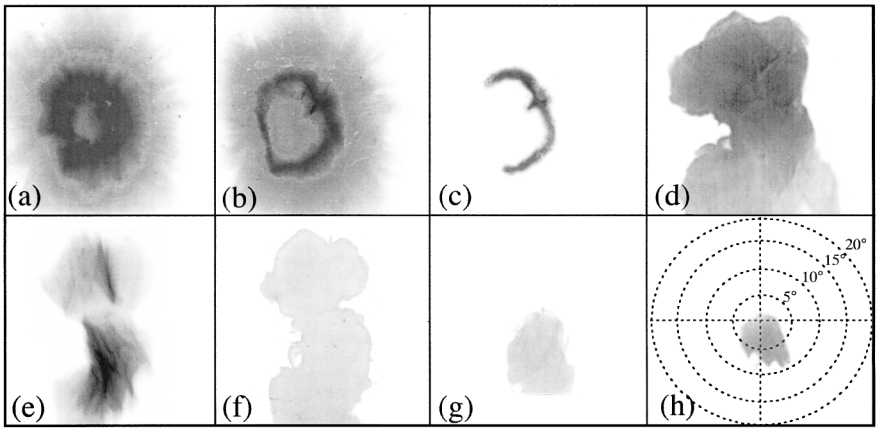

FIG. 5. Radiochromic film/CR39 detector package. (a) RCF [proton energy (E) < 3 MeV]; (b) RCF ($E \sim 4$ MeV); (c) CR39 ($E \sim 4$ MeV); (d) CR39 ($E \sim 11$ MeV); (e) RCF ($E \sim 13$ MeV); (f) CR39 ($E \sim 13$ MeV); (g) CR39 ($E \sim 18$ MeV); (h) CR39 ($E \sim 20$ MeV). The horizontal axis in (h) is the plane of propagation of the laser.

also been previously observed in longer pulse experiments where they were inferred to be formed by nonuniformities in the laser spot [21].

The higher-energy component of the ion emission appears to be qualitatively different from the lower-energy component and does not exhibit a ring structure. It is probable that the initial acceleration of these ions occurs near the critical surface. The ponderomotive force of the focused laser light can cause charge separation and ion acceleration [11], and it is likely that this is the source of the angular emission pattern of the accelerated high-energy protons [Figs. 5(d), 5(f)–5(h)]. The laser is incident onto the target at a 45° angle to the target normal so that on average, the direction of accelerating electric fields created by charge separation is normal to the surface. However, the resulting "Coulomb explosion" can also accelerate ions out of this plane, which is evident in Fig. 5 where the major component of the higher-energy proton emission is directed above and below the laser plane. Note, however, that it is unlikely that all of the energy of these protons is produced via charge separation induced by the laser field. It is probable that electrostatic fields due to the escaping hot electrons also contribute significantly to the energy of the observed accelerated ions since the ponderomotive energy of the laser pulse (at $I \sim 5 \times 10^{19}$ W/cm^2) should contribute only a few MeV to the energy of the protons. The qualitative change between high- and low-energy protons is also evident in the spectrum of Fig. 3.

In conclusion, the first detailed measurements of the energy spectra of protons and heavy ions emitted from the front of a solid target during ultrahigh intensity interactions have been performed. These experiments suggest that these are two components to the accelerated proton and ion population. The lower-energy part is formed as the heated plasma ablates and is strongly influenced by the magnetic field generation in the plasma. In contrast, it is likely that the highest-energy components are initially accelerated during the laser interaction period by electrostatic fields created by charge separation. These measurements record the highest energy ions from a laser-plasma interaction with energies of lead ions up to 430 ± 40 MeV.

A potential application could be as an ion source for heavy-ion accelerators [22]. Such accelerators require $\sim 10^{10}$ highly stripped ions with energies of a few MeV/nucleon and an average current of 10 mA. The source described in this paper could be suitable and may overcome the need for a "preinjector" as used in current technology.

We would like to acknowledge useful discussions with Dr. K. W. D. Ledingham and the technical assistance of the VULCAN operations team. This work was supported by the United Kingdom Engineering and Physical Sciences Research Council.

[1] D. Gordon *et al.,* Phys. Rev. Lett. **80**, 2133 (1998); E. Esarey *et al.,* IEEE Trans. Plasma Sci. **24**, 252 (1996).
[2] E. L. Clark *et al.,* Phys. Rev. Lett. **84**, 670 (2000).
[3] M. Borghesi *et al.,* Phys. Rev. Lett. **81**, 112 (1998).
[4] L. Gremillet *et al.,* Phys. Rev. Lett. **83**, 5015 (1999).
[5] M. Tabak *et al.,* Phys. Plasmas **1**, 1626 (1994).
[6] D. W. Forslund *et al.,* Phys. Rev. Lett. **48**, 1614 (1982).
[7] A. P. Fews *et al.,* Phys. Rev. Lett. **73**, 1801 (1994); F. N. Beg *et al.,* Phys. Plasmas **4**, 447 (1997).
[8] R. L. Carlson *et al.,* IEEE J. Quantum Electron. **17**, 1662 (1981).
[9] S. J. Gitomer *et al.,* Phys. Fluids **29**, 2679 (1984).
[10] T. Tan *et al.,* Phys. Fluids **27**, 296 (1984).
[11] K. Krushelnick *et al.,* Phys. Rev. Lett. **83**, 737 (1999).
[12] C. N. Danson *et al.,* J. Mod. Opt. **45**, 1653 (1998).
[13] Y. Kishimoto *et al.,* Phys. Fluids **26**, 2308 (1983).
[14] L. M. Wickens *et al.,* Phys. Rev. Lett. **41**, 243 (1978).
[15] M. H. Key *et al.,* Phys. Plasmas **5**, 1966 (1998).
[16] M. I. K. Santala *et al.,* Phys. Rev. Lett. **84**, 1459 (2000); P. A. Norreys *et al.,* Phys. Plasmas **6**, 2150 (1999).
[17] W. L. McLaughlin *et al.,* Nucl. Instrum. Methods Phys. Res., Sect. A **302**, 165 (1991).
[18] J. A. Stamper *et al.,* Phys. Rev. Lett. **26**, 1012 (1971).
[19] M. Tatarakis *et al.,* Phys. Rev. Lett. **81**, 999 (1998).
[20] L. Gremillet, in *Proceedings of the Third International Workshop on the Fast Ignition of Fusion Targets* (RAL Technical Report No. RAL-TR-1998-085, 1999).
[21] E. F. Gabl *et al.,* Phys. Rev. Lett. **63**, 2737 (1989).
[22] H. Haseroth and H. Hora, Laser Part. Beams **14**, 393 (1996).